



**HAL**  
open science

## Design of a set-up for measuring the residual compressive strength after high load and high cycle compression fatigue on CFRP

A. Launay, V. Keryvin, J.-C. Grandidier, P.-Y. Mechin, R. Balze

### ► To cite this version:

A. Launay, V. Keryvin, J.-C. Grandidier, P.-Y. Mechin, R. Balze. Design of a set-up for measuring the residual compressive strength after high load and high cycle compression fatigue on CFRP. *Composite Structures*, 2022, 286, pp.115294. 10.1016/j.compstruct.2022.115294 . hal-03830296

**HAL Id: hal-03830296**

**<https://hal.science/hal-03830296>**

Submitted on 22 Jul 2024

**HAL** is a multi-disciplinary open access archive for the deposit and dissemination of scientific research documents, whether they are published or not. The documents may come from teaching and research institutions in France or abroad, or from public or private research centers.

L'archive ouverte pluridisciplinaire **HAL**, est destinée au dépôt et à la diffusion de documents scientifiques de niveau recherche, publiés ou non, émanant des établissements d'enseignement et de recherche français ou étrangers, des laboratoires publics ou privés.



Distributed under a Creative Commons Attribution - NonCommercial 4.0 International License

# Design of a set-up for measuring the residual compressive strength after high load and high cycle compression fatigue on CFRP

A. Launay<sup>a,b</sup>, V. Keryvin<sup>a,\*</sup>, J.-C. Grandidier<sup>c</sup>, P.-Y. Mechin<sup>d</sup>, R. Balze<sup>b</sup>

<sup>a</sup>Univ. Bretagne Sud, UMR CNRS 6027, IRDL, F-56321 Lorient, France

<sup>b</sup>GSea Design, F-56100 Lorient, France

<sup>c</sup>ISAE-ENSMA, UPR CNRS 3346, PPrime, F-86360 Chasseneuil-du-Poitou, France

<sup>d</sup>Dassault Systèmes, Catia Composites, F-78140 Velizy-Villacoublay, France

---

## Abstract

A new testing set-up to measure the compressive strength of continuous fibre composite materials (CFRP) under both static and fatigue loadings is described. A specific symmetric sandwich beam with CFRP face sheets is used with a four-points bending set-up. Its mechanical design is carried out by fine Finite Element Analyses (FEA) to ensure that the failure mode is axial compression by fibre micro-buckling. Precise comparisons between numerical simulations and experimental quasi-static experimental results are found to be sound, validating the FEA model. The latter is used to design the sandwich beam in terms of strength and stability criteria. Finally, a high cycle fatigue campaign ( $10^7$  cycles) with high modulus CFRP skins demonstrates the performance of the set-up. Repeatable results and acceptable failure modes are obtained.

**Keywords:** Compressive strength; Fatigue; Testing set-up; High modulus carbon fibre; Composite materials

---

\*Corresponding author: [vincent.keryvin@univ-ubs.fr](mailto:vincent.keryvin@univ-ubs.fr)  
Preprint submitted to *Composite Structures*

December 17, 2021

## 1. Introduction

Continuous fibres composite materials, and more particularly Carbon Fibre Reinforced Plastics (CFRP), continue to see their use grow in many sectors such as aeronautics, aerospace and car racing sports. They allow the construction of lightweight, resistant structures with optimised stiffness.

A problem that generated a lot of studies since the 1980s is the measurement of compressive strength [1, 2, 3]. It is generally accepted that the compressive strength of unidirectional plies (UD) is much lower than their tensile strength [5]. This mechanical property is often the one that dictates the design of structures. This is particularly the case on slender structures, loaded in compression or bending. We can take as an example an airplane wing or a sailboat mast. It is important to highlight that most of the time and particularly in the case of the preceding examples, the loads applied to these structures vary over time and can be assimilated to cyclic loadings.

Under these conditions, designers must be able to use accurate data regarding the compressive strength of the CFRP. They must therefore know the evolution of the compressive strength after cyclic loading with the aim to guarantee the integrity of the structure over its entire service life.

The characterisation of the compressive strength of CFRP has been the subject of intense debate for many years due to the specificity of the microscopic failure mechanism. Indeed, the compressive failure of CFRPs is caused by an instability known as micro-buckling. As early as the 1980s, it was noted that in most cases, strength measurements obtained by pure compression tests led to significant dispersion. Although many efforts have been made over the last thirty years to improve experimental techniques, it appears that results are highly dependent on different factors such as the

machining of the specimens, the type of experimental set-up (stress concentration, buckling), load introduction (shear loading, end loading, mixed loading) and the skills of the experimenter. These issues are even more exacerbated with compression/compression fatigue testing and the cause of degradation or failure is all the more difficult to discern [14]. As a first approximation, pure compression tests generate a constant compression state. Yet, singularities linked to the test set-up may have a considerable influence on the fracture mechanisms. Close to these singularities (grips, anti-buckling devices. . .) the compression stress is burdened by strong gradients depending on the set-up precision and design.

To solve these problems, several authors have proposed alternatives [7, 8, 9]. Four-points bending tests and pinned-end buckling tests circumvent this bias. A common alternative is to use a four-point bending device on monolithic samples [10]. The use of this solution was motivated by the difficulty of carrying out a pure compression test without parasitic components and without local stress concentrations. If these set-ups nevertheless generate stress gradients, these latter are imposed and quantifiable by calculation. When these tests are correctly designed, fractures occur far from where loading is introduced, and measurements correspond to what is expected and sought from the material.

The four-point bending device has the advantage to provide a large area where the deformation field is homogeneous and in pure bending. It gives the possibility of a precise and reliable measurement of the modulus of elasticity during loading and permits to calculate the compressive strength [11]. However, four-point bending devices generate gradients in the thickness and Drapier et al. [12] have shown that the compressive strength value has

a part related to the configuration of the tested structure: the structural effect. They showed the dependence on three main parameters: the consecutive thickness of UD plies [10], the strain gradient and the orientation of neighbouring off-axis plies of the UD [13]. It is very difficult to limit the contribution of these parameters, but some configurations allow it. This is the case for sandwich structures which, depending on their design, can limit structural effects (small deformation gradient in the skins). Indeed, taking the same imposed moment and the same thickness for a given composite laminate, skins of sandwich samples lessen the stress gradient effect with respect to a monolithic sample. In both cases a structural effect exists but is quantifiable and its participation to the compression fracture mechanisms is largely documented. Sandwich beams are classically (ASTM D5467) made with a compressively loaded face sheet of lower thickness. As stated by Baumann and Hausmann [14] in their recent review work on the compression fatigue testing set-ups, the extension of the use of sandwich beams to fatigue testing has not been reported in literature.

The objective of this paper is to propose an experimental set-up dedicated to *axial compression fatigue testing of CFRP based on symmetric sandwich beams*. This set-up should be able to impose compression-compression fatigue loading, over a high number of cycles (millions or tens of millions) and with very high loads (since in quasi-static loading, the behaviour is reversible up to 90% of the strength [5]), without any possible damage other than in the studied area of the tested structure. A careful design is however necessary to ensure that compressive damage occur and the proper compressive failure mode of the studied unidirectional ply is triggered, without any other instability modes. As stated by Seemann [15], a detailed fi-

nite element analysis is required in this situation. Therefore, after describing clearly the specifications of the design, this numerical model will be presented. Then, we will carry out an experimental validation by quasi-static testing and a confrontation with the numerical model. Eventually, the final validation of the test fixture will be made through an experimental campaign in compression-compression fatigue loading with emphasis on the evolution of the residual compressive strength. The experimental results will be compared to literature which is rather sparse on this very topic [16, 17]. We will focus on the case of high modulus carbon fibres of high interest in marine engineering for masts and hydrofoils, for example [18], which is even less addressed.

## **2. Description of the experimental set-up**

### *2.1. Specifications*

The objective is to propose an experimental device dedicated to the study of compressive strength during and after compressive fatigue. The dispersions induced by the experimental device and the placement of the specimen must be reduced as much as possible. In addition, the test device must allow the specimen to reach both compressive failure and cycling at a high stress level, close to static failure. It must be possible to cycle over many cycles, which means that no damage must occur outside the study area. Therefore, the test device must not induce any parasitic friction. The study area must be sufficiently large and may be subjected, as much as possible, to the purest compressive stress state. The design of the device must allow the structural effects to be known as much as possible while having a stack-

ing, particularly concerning the orientation of the off-axis plies, representative of the stacks used in yacht racing.

## 2.2. Geometry

In this paper the 4-point bending test was chosen (Figure 1). Its geometry was adapted to have a sufficiently large area between internal loading rollers (approx. 2500 mm<sup>2</sup>) and appropriate safety coefficients for the shear stress areas to avoid other modes of failure. Pads were used to convert the linear surface stress between the loading rollers and the specimen. They are 3 mm thick and are made of polyethylene to limit friction. A sandwich beam was used to reduce the gradient in the UD plies in compression. With this configuration, between loading rollers, one skin is in almost pure compression while the other is in almost pure tension. These skins are identical and consist in the following stacking: [+45°(150 g/m<sup>2</sup>) | -45°(150 g/m<sup>2</sup>) | 0<sub>2</sub>°(300 g/m<sup>2</sup>)]<sub>s</sub>. Their thickness is 1.85 mm each. This configuration limits the strain gradient in UD plies. The thickness of each block of plies were measured by optical microscopy. The four UD have a total thickness of 1.28 mm, the ± 45° plies on the outside facing of the specimen have an average thickness of 0.27 mm and the ± 45° plies on the inside facing of the specimen have an average thickness of 0.3 mm. This slight difference is related to the manufacturing process of the skins (compaction). Figure 1 is an illustration of the test set-up and its main geometrical dimensions.

## 2.3. Materials

The skins are manufactured with prepreg plies with high modulus carbon fibres from Mitsubishi (HR40, volume fraction of 52 %) with an axial stiffness around 360 GPa [18] and epoxy resin system from Structil (R367-2)

with a low glass transition temperature (120°C). The core has been chosen from those usually employed in the nautical sector. It consists of two distinct areas. The first zone is composed only of Nomex®, supplied by Hexcel under the reference HRH-10-4.8-48. This area is 60 mm in length, centred lengthwise in relation to the centre of the specimen and extends across the width. It provides a core with sufficient high properties to prevent buckling of the skins, while limiting perturbations to the local fields, as would have been the case with a core having higher properties. The second area, in the arms and under the loading rollers, is made from the same Nomex® which has been immersed in a low-density mixed filled resin insert (ISOBOND SR1252 + KTA313). This provides a core with significantly higher properties, especially shear properties.

The properties of the UD ply and the Nomex® paper are reported in Table 1. The  $E_1$  modulus of UD ply (in fiber direction) and  $E_2$  modulus of the Nomex® paper (cell height direction) were calculated by an inverse method based on the numerical model and the mechanical tests, presented in § 3.2 and in § 4.1, respectively. The other properties of UD ply are obtained by standard analytical homogenisation methods and those of Nomex® paper are obtained from Refs. [19, 20]. The orientation of the material coordinate system corresponds to that usually used for this type of anisotropic material [21]. For the rollers (steel) and the pads (polyethylene) the properties of the materials are reported in Table 2. The specimens were manufactured by Multiplast company (Carboman group, Vannes, France). The components were cured separately in an oven (unassembled) and then the assembly of the skins and the core was carried out using a film of Hexcel ST1035 glue (300 g/m<sup>2</sup>). An additional curing in the oven is then neces-

sary to ensure the bonding of these elements. This method limits the phenomenon of telegraphing [15] and allows good control of the geometry and more specifically the thickness. Plates were machined by waterjet cutting into  $600 \times 30 \times 16.6 \text{ mm}^3$  samples.

### **3. Mechanical design and validation of the experimental set-up**

The system presented must ensure that the failure of the structure is caused by the failure of the skin in compression. Thus, particular attention will be paid to the mechanical strength of the core and to local buckling problems to avoid any other failure modes.

#### *3.1. Design criteria*

##### *3.1.1. Core*

The four-point bending set-up induces mainly two types of force components that can be critical in the core. Firstly, compressive stresses are introduced under the loading rollers, in the direction of loading ( $\sigma_{YY}$  - Fig. 1). In this area, the core is made of Nomex® and mixed filled resin insert. Compressive stresses are also present in the central zone, mainly in two directions X and Y (Fig. 1), where the core is made of Nomex® only. Shear forces between the outer and inner rollers are also generated. It was to deal with this problem that the choice was made to reinforce this area by embedding the Nomex® in a mixed filled resin insert. Thus, for a given section, the latter occupies the majority of the surface and will therefore support the majority of the shear forces. Based on this information, the stresses obtained with the finite element model will be compared to the maximum allowable stresses to evaluate the integrity of the structure in each of these

zones and for each of these stress components. The compressive and shear strength properties of the mixed filled resin insert are presented in Table 3. These properties come from the supplier's data sheet [22]. The strength properties, considering the anisotropy of Nomex® paper, are also presented in Table 3. They are based on the work of Seemann [15].

### *3.1.2. Face wrinkling*

Sandwich beams can be subject to buckling failure modes. In the case of this configuration, the most likely mode is face wrinkling. The buckling of the structure is a sudden phenomenon and occurs in the same area as the compressive failure. Thus, it could be difficult to identify precisely after failure, whether it is a compression failure mode or a buckling mode that has subsequently led to a compression failure. It is therefore important to consider this possibility of a buckling failure mode in design. This will be the subject of specific finite element analyses. The minimum acceptable safety factor has been set at 1.2.

## *3.2. Numerical validation*

### *3.2.1. Model description*

To evaluate the proposed experimental set-up, a finite element model of the four-point bending test was built using the commercial Finite-Element code Abaqus™ v. 6-14 (Dassault Systèmes). This simulation assumes a non-deformable test device, so only the components shown in Figure 1 are modelled. As buckling is one of the main issues for sandwich beams, the assumption of symmetry was avoided, especially in the middle area of the specimen, to capture all possible buckling modes. Thus, the specimen is fully modelled. The model contains skins modelled as linear shell elements

with four nodes, four integration points in the plane and three integration points in the thickness of each ply of the laminate. The two core components (Nomex® and mixed filled resin insert) are each modelled in a specific way: i) the mixed filled resin insert in the areas outside the loading rollers is modelled by linear volume elements with 8 nodes and 8 integration points; ii) the Nomex®, present along the entire specimen length, has all its cells modelled. Indeed, as explained by Seemann [15], this is the only way to capture possible buckling of cell walls. Linear four-node shell elements with four in-plane and three through thickness integration points were used.

The assumption of a “perfect” assembly is imposed by the model. The adhesion of the Nomex® with the mixed filled resin insert, as well as the glue fillet created during the assembly of the skins with the core, are therefore not modelled. Hence, this model does not allow us to observe any issues with debonding between the components of the specimen. The different components, then the specimen, are shown in Fig. 2.

This “perfect” assembly resulted in a continuous mesh of the whole specimen with coincident nodes between all the components of the structure. This modelling without connectors and with interfacial continuity, as well as the choice of elements with the same degree of interpolation and complete integration, favours the accuracy of the result from a kinematic point of view. Frictionless contact was considered between the rollers and the pads and between the pads and the specimen.

The UD plies were considered to have a transverse isotropic behaviour with a non-linear elasticity in the fibre direction. The modelling of this behaviour

was introduced as in Wisnom [23] according to Eq. (1):

$$E_1(\epsilon_L) = E_1^{\text{initial}} + k\epsilon_L \quad (1)$$

where  $E_1$  is the UD axial modulus,  $E_1^{\text{initial}}$  its initial value,  $\epsilon_L$  the axial strain and  $k = \alpha$  if  $\epsilon_L < 0$  or  $k = \beta$  if  $\epsilon_L > 0$ .

The  $\beta$  parameter has a value of 24 GPa/% and the  $\alpha$  parameter has a value of 38 GPa/%. They were identified by the method described by Keryvin et al. [11] during a four-point bending campaign on monolithic specimens of the same material (R367-2/HR40).

### 3.2.2. Margin of safety for the core

A detailed verification of the safety factors in the core was carried out. Figure 3 shows some examples of stress distribution in the core components. Table 4 indicates that the lowest safety factor is for the compression failure of Nomex® paper, with a safety factor of 2. Figure 3 indicates that the critical area where this factor occurs is in the centre of the specimen (purple ellipse), just below the skin in compression. Considering all these information, the simulation suggests that the failure of the specimen will not be caused by the failure of the core. In fact, when the compression skin failure occurs in the upper skin, the minimum safety factor on the core is approximately 2.

### 3.2.3. Verification of the face wrinkling safety factor

The buckling calculation is carried out in two steps. First, an initial displacement is applied: this is a pre-buckling step that allows nonlinearities to be considered. Then, an instability calculation is performed from the previ-

ous strain state using the “Subspace” method implemented in Abaqus™. The first buckling mode found is the face wrinkling type and is shown in Fig. 4 (skins not shown). A sensitivity to the initial displacement was carried out and it was found that the evolution of the critical buckling displacement became negligible from an initial displacement of -10 mm, so this value was used. The critical buckling displacement is found to be -17.8 mm for a compressive stress in the outermost UD of -1190 MPa. This type of UD has a strength of about 950 MPa (see § 4.3), so the buckling safety factor is about 1.25, higher than the minimum criterion of 1.2 set in § 3.1.2. Note that the stress is calculated by means of the numerical model. The stress is linear in each ply because of the constant deformation gradient and what we mean by a “compressive stress in the outermost UD” is the stress at the upper edge of this very ply where it is the higher. In this section, the results of the numerical simulation of the most critical points were presented. They allow to exclude a core failure as well as a face wrinkling. The overall safety factor is of the order of 1.25.

#### **4. Experimental validation and confrontation with the numerical model**

##### *4.1. Identification of quasi-static failure mode*

To confirm the failure mode, quasi-static tests were carried out at 5 mm/min on eight specimens including three fully instrumented ones. A universal testing machine (Instron 5969, 50 kN load cell) was used. Mono-axial strain gauges (10 mm length - 120  $\Omega$  - Kyowa) were glued on both the compression and the tension sides, in the middle of specimen. An extensometer system was installed to calculate the maximum deflection. A Mistras acoustic

emission (AE) system with preamplifiers (40 dB) in connection with resonant R15 transducers was used. Transducers were positioned on the compression skin at 200 mm from each other, centered on the middle of the specimen. The complete instrumentation is shown in Fig. 5.

To get additional information about the mechanisms leading to failure and to confirm the absence of damage prior failure, load and unload cycles were carried out with increasing intensities. The different cycles are defined by maximum load reached and are presented in Table 5.

For sake of clarity, only the graphs of one of the three fully instrumented test specimens will be shown here. Figure 6 represents the main signals of load (F), displacement (U) and longitudinal strain ( $\epsilon_L$ ) of the specimen HR7\_1. Only the three most important cycles are shown. It is found that successive loadings do not change the behaviour of the structure, even when exceeding 90 % of failure load. This result suggests that no damage has developed or is very low. A very slight hysteresis is visible on the Fig. 6 (b) when the load is greater than - 3000 N. However, successive loading paths are almost identical, demonstrating the reversible nonlinear behaviour of this composite in compression. As the hysteresis was observed without significant acoustic emission signals (presented below), this phenomenon can be explained by the presence of low friction in the experimental device. As in the analysis of monolithic specimens proposed in Ref. [11], the indicator  $\lambda$  is defined by Eq. (2) where t is the thickness of the sandwich.

$$\lambda = \frac{t}{2} \frac{\epsilon_c + \epsilon_t}{\epsilon_c - \epsilon_t} \quad (2)$$

In Ref. [11], it represents the offset of the neutral fibre with respect to the

median plane, in the thickness of the specimen. In our case, it allows to combine the strain of the compression skin and the tension skin within the same indicator and thus accentuates the differential between them. Fig. 6 (d) represents the evolution of the indicator  $\lambda$  as a function of the longitudinal strain measured on compression skin ( $\epsilon_c$ ) and on tension skin ( $\epsilon_t$ ). There is a point of intersection between the loading and unloading path, which is constant. This one appears for a longitudinal strain around  $-3800 \mu\text{m/m}$ , which corresponds to approximately  $-3200 \text{ N}$ . This coincides with the appearance of the hysteresis on Fig. 6 (b). The invariance of this intersection point reinforces the assumption of low mechanical friction within the experimental setup. These graphs are representative of all three fully instrumented specimens that were tested.

The main acoustic emission signal records are shown in Fig. 7. Very limited events were detected, confirming the very low level of damage before failure suggested by the global response. The Kaiser effect [24] is diffuse, probably due to the limited mechanical friction inducing an increase in the number of hits during loading and unloading.

The observation of the different fracture surfaces of the specimens (cf. Fig. 8) has confirmed that the specimens fractured by a failure of their skin in compression. Indeed, kinking bands could be observed, characteristic of a compressive failure. The measured kinking band angles are in agreement with those found in the literature [25, 26] and are located in the out of plane direction. However, it cannot be excluded that there are also in-plane kinking bands. According to the configuration, those can be more difficult to identify.

All observations and measurements made during this campaign validate the

device for the characterization of the compressive strength of high modulus carbon/epoxy UD under static conditions.

#### *4.2. Confrontation of numerical results to experiments*

Simulation results are compared with the experimental signals of the last cycle of each specimen in Fig. 9. The correlation is very good, both validating the numerical model and giving credit to the design of the core and the addition of pads in the contact areas. The trend of the indicator  $\lambda$  is also good; differences at the beginning of the curves are due to strain gauge measure dispersion for small strains.

#### *4.3. Study of residual strength after fatigue*

Twenty-seven specimens were cycled to challenge the experimental set-up under cycling loading and to study the evolution of the residual strength after fatigue. An ElectroPuls Instron E10000 was used (7 kN load cell). No specific instrumentation was used for these tests.

First, eight specimens were tested in quasi-static mode giving the compressive strength before fatigue:  $X_C^0 = 960 \pm 67$  MPa. The specimens had no visible defects, and the standard deviation is of similar order as the 4-point bending tests on monolithic structures usually carried out in yacht racing [18, 27, 28]. Failure was defined in the numerical model when the strain in the outermost 45° ply (compression face) matched the strain measured experimentally by the strain gauge on compression face at failure.

The specimens were cycled and then, for those that did not fail during cycling (most cases), a quasi-static test was used to estimate their post-fatigue residual strength. In all cases, the numerical model is used to obtain a stress at failure since this model is the best estimation of the strain gradient in

the skin and thus allows the most reliable estimation of the strain in the outermost UD ply. As the specimens used in the initial static tests were equipped with strain gauges (in the centre of each of the outer faces), these signals were used as a reference for the model. As these specimens were not equipped with strain gauges, the force signal was used to adjust the numerical model. This signal was first corrected for each specimen to consider the deviation of its width from the model (width:  $28 \pm 1$  mm). No decrease in stiffness was observed on two specimens that had been cycled to the maximum number of cycles in this fatigue campaign ( $1.10^7$  cycles – unfractured specimen). The use of the force signal to calibrate the numerical model at failure was therefore considered acceptable for extract the residual strength at failure load ( $X_C^{res}$ ). This residual strength is then compared to the average strength calculated from the quasi-static tests.

For all these tests, the load ratio during cycling is  $R = 1.3$  (compression-compression) and the loading frequency is 10 Hz. The maximum stress level ( $\sigma_{max}$ ) is 76 % of static compressive strength  $X_C^0$ . The number of cycles is between  $10^5$  and  $10^7$  cycles.

Fatigue campaign results are shown in Fig. 10. It is observed that at this stress level, the compressive residual strength is similar to the average compressive strength observed on the batch before fatigue ( $X_C^0$ ). The average residual compressive strength even appears to increase for specimens that have been stressed beyond one million cycles. These observations are in line with those of Bech et al. [17] and Shokrieh and Lessard [16] on AS4/3501-6 specimens, tested with a pure compression set-up. It is noted that the standard deviation for residual strength is about 20% higher than the quasi-static mode. These experiments validate the capacity of the experimental

test fixture for studying the influence of cycling on the evolution of the residual compressive strength under high load and for a large number of cycles.

Baumann and Hausmann [14], reporting that fatigue compression testing on CFRP sandwich beams had not been proposed yet, pointed out issues such as the need to know the fatigue failure modes before testing. In our case, no fatigue damage was noticeable. Should it has been the case, the use of the detailed FEA model would make it possible to take it into account.

## **5. Conclusion**

We have discussed in this paper the characterisation of carbon/epoxy UD in fibre direction, in compression, a challenging problem especially under fatigue loading. In this paper, a testing set-up to study the evolution of compressive residual strength in fibre direction, after compression fatigue, of high modulus carbon/epoxy UD is proposed. Its relevance was verified by using a sufficiently accurate finite element model and by an experimental campaign. The correlation between the model and the quasi-static tests was excellent. A fatigue campaign was also carried out and showed that the test fixture could be used to load a structure in compression over a very large number of cycles, but also under very high stress levels. No degradation of the compressive residual strength after fatigue was observed. This validates the design of the whole test set-up and seems to be in agreement with the fatigue results in literature indicating that high performance CFRP show little or no degradation of their compressive residual strength over the cycles, even under high stress levels. The design of the test fixture thus fulfils

its objective: to study the evolution of the compressive residual strength after fatigue under high stress level and a large number of cycles, for CFRP with high modulus carbon fibres. Pure compression tests could also have been performed. However, some shortcomings have been reported in literature, including stress concentrations in the clamping grips or friction with the anti-buckling devices. During fatigue testing, these pure compression set-ups will result in damage. Four-points bending set-ups are more appropriate even if they require specific instrumentation and more complicated data analysis. Meanwhile, this permits to induce a fatigue loading without any influence of the set-up and therefore, in turn, to measure the residual properties of the studied material. The objective of this study was to assess this possibility. Should other composites be tested with other stiffnesses, numerical simulation would be employed. Yet, in a future work, a parametric study will make it possible to create charts or plots linking the test parameters to a large range of composites stiffnesses. Finally, since this set-up creates in a symmetric way a deformation gradient in compression and tension. Therefore, it is indeed possible to extend this fatigue loading to the tensile behaviour when this one has properties in strength lower than in compression such as cementitious materials [29].

### **Acknowledgements**

We would to thank the French ANRT for partial funding of the PhD grants of A. Launay (# 2017/0421) and P-Y. Mechin (# 2012/1621). Encouraging discussions with Dr. P. Davies (Ifremer), Prof. C. Baley (UBS) and Dr. D. Cartié (Coriolis Composites) are also acknowledged. The experimental contributions of F. Portanguen, H. Bellegou, A. Le Palabe and K. Henry (UBS)

are finally acknowledged.

### Data availability

The raw/processed data required to reproduce these findings cannot be shared at this time due to technical or time limitations.

### References

- [1] D. H. Woolstencroft, A. R. Curtis, and R. I. Haresceugh. A comparison of test techniques used for the evaluation of the unidirectional compressive strength of carbon fibre-reinforced plastic, 1981. ISSN 00104361.
- [2] T. A. Bogetti, J. W. Gillespie, and R. B. Pipes. Evaluation of the IITRI compression test method for stiffness and strength determination. *Composites Science and Technology*, 32(1):57–76, 1988. ISSN 02663538. doi: 10.1016/0266-3538(88)90029-2.
- [3] O. Anthoine, J. C. Grandidier, and L. Daridon. Pure compression testing of advanced fibre composites. *Composites Science and Technology*, 58(5):735–740, 1998. ISSN 02663538. doi: 10.1016/S0266-3538(97)00158-9.
- [4] AGARD-R-785. The Utilization of Advanced Composites in Military Aircraft. Technical Report April, 1992.
- [5] O. Allix, P. Ladevèze, and E. Vittecoq. Modelling and identification of the mechanical behaviour of composite laminates in compression. *Composites Science and Technology*, 51(1):35–42, 1994. ISSN 02663538. doi: 10.1016/0266-3538(94)90154-6.
- [14] A. Baumann, and J. Hausmann. Compression Fatigue Testing Setups for Composites—A Review. *Advanced Engineering Materials*, 23(2):2000646, 2021. doi: 10.1002/adem.202000646.
- [7] M. R. Wisnom. On the high compressive strains achieved in bending tests on unidirectional carbon-fibre/epoxy. *Composites Science and Technology*, 43(3):229–235, 1992. doi: 10.1016/0266-3538(92)90093-1.
- [8] O. Montagnier and C. Hochard. Compression characterization of high-modulus carbon fibers. *Journal of Composite Materials*, 39:35–49, 2005. doi: 10.1177/0021998305046433.

- [9] F. Laurin, P. Paulmier, and F. X. Irisarri. Determination of the longitudinal compressive strength of a CFRP ply through a tensile test on a laminate. *Composites Part A: Applied Science and Manufacturing*, 113:209–219, 2018. doi: 10.1016/j.compositesa.2018.07.026.
- [10] M. R. Wisnom. The effect of specimen size on the bending strength of unidirectional carbon fibre-epoxy. *Composite Structures*, 18(1):47–63, 1991. doi: 10.1016/0263-8223(91)90013-O.
- [11] V. Keryvin, A. Marchandise, P. Y. Mechin, and J. C. Grandidier. Determination of the longitudinal non linear elastic behaviour and compressive strength of a CFRP ply by bending tests on laminates. *Composites Part B: Engineering*, 187:107863, 2020. doi: 10.1016/j.compositesb.2020.107863.
- [12] S. Drapier, J.-C. Grandidier, and M. Potier-Ferry. Towards a numerical model of the compressive strength for long fibre composites. *European Journal of Mechanics - A/Solids*, 18(1):69–92, jan 1999. doi: 10.1016/S0997-7538(99)80004-7.
- [13] J.-C. Grandidier, G. Ferron, and M. Potier-Ferry. Microbuckling and strength in long-fiber composites: theory and experiments. *International Journal of Solids and Structures*, 29(14-15):1753–1761, 1992. doi: 10.1016/0020-7683(92)90168-S.
- [14] A. Baumann and J. Hausmann. Compression Fatigue Testing Setups for Composites—A Review. *Advanced Engineering Materials*, 23(2):2000646, 2021. doi: 10.1002/adem.202000646.
- [15] R. Seemann. *A Virtual Testing Approach for Honeycomb Sandwich Panel Joints in Aircraft Interior*. 2020. doi: 10.1007/978-3-662-60276-8.
- [16] Mahmood M. Shokrieh and Larry B. Lessard. Progressive fatigue damage modeling of composite materials, Part I: Modeling. *Journal of Composite Materials*, 34(13), 2000. doi: 10.1106/NCNX-DXP1-JT6A-E49E.
- [17] J. I. Bech and S. Goutianos and T. L. Andersen and R. K. Torekov and P. Brøndsted A New Static and Fatigue Compression Test Method for Composites. *Strain*, 47(1):21–28, 2000. doi: 10.1111/j.1475-1305.2008.00521.x.
- [18] P. Y. Mechin, V. Keryvin, J. C. Grandidier, and D. Glehen. An experimental protocol to measure the parameters affecting the compressive strength of CFRP with a fibre micro-buckling failure criterion. *Composite Structures*, 211:154–162, 2019. doi:

- 10.1016/j.compstruct.2018.12.026.
- [19] R. Roy, K. H. Nguyen, Y. B. Park, J. H. Kweon, and J. H. Choi. Testing and modeling of Nomex™ honeycomb sandwich Panels with bolt insert. *Composites Part B: Engineering*, 56:762–769, 2014. doi: 10.1016/j.compositesb.2013.09.006.
- [20] R. Roy, S. J. Park, J. H. Kweon, and J. H. Choi. Characterization of Nomex honeycomb core constituent material mechanical properties. *Composite Structures*, 117(1): 255–266, 2014. doi: 10.1016/j.compstruct.2014.06.033.
- [21] D. Gay, S.V. Hoa, and S.W. Tsai. *Composite materials: Design and applications*. 3rd edition, 2002. ISBN 9781420031683.
- [22] Sicomin. IsoBond SR 1252 / KTA 31x Mousse syntactique basse densité, 2014. URL [http://www.sicomin.com/datasheets/product-pdf\\_{\\_}fr209.pdf](http://www.sicomin.com/datasheets/product-pdf_{_}fr209.pdf).
- [23] M. R. Wisnom. The effect of fibre misalignment on the compressive strength of unidirectional carbon fibre/epoxy. *Composites*, 21(5):403–407, 1990. doi: 10.1016/0010-4361(90)90438-3.
- [24] J. Kaiser. *Untersuchungen über das Auftreten von Geräuschen beim Zugversuch*. PhD thesis, Technische Hochschule München, 1950.
- [25] R. Effendi. Compressive Behaviour of Unidirectional Carbon/Epoxy Composites. *Advanced Composites Letters*, 2(4):096369359300200, jul 1993. doi: 10.1177/096369359300200405.
- [26] A. Jumahat. *Effect of nanofillers on thermo-mechanical properties of polymers and composite laminates*. PhD thesis, University of Sheffield, UK, 2011.
- [27] P.-Y. Mechin, V. Keryvin, and J.-C. Grandidier. *Limitations on adding nano-fillers to increase the compressive strength of continuous fibre / epoxy matrix composites*. *Composites Science and Technology*, 192:108099, 2020. doi: 10.1016/j.compscitech.2020.108099.
- [28] P.-Y. Mechin, V. , and J.-C. Grandidier. *Effect of the nano-filler content on the compressive strength of continuous carbon fibre/epoxy matrix composites*. *Composites Part B: Engineering*, 224:109223, 2021. doi: 10.1016/j.compositesb.2021.109223.
- [29] B.-T. Huang, Q.-H. Li, and S.-L. Xu , *Fatigue Deformation Model of Plain and Fiber-Reinforced Concrete Based on Weibull Function*. *Journal of Structural Engineering*, 145(1):04018234, 2019. doi: 10.1016/j.compstruct.2014.06.033.

**Table 1.** Elastic properties of UD ply and Nomex® paper (transverse isotropy). 1 is the fibre direction for the UD while 2 is the height direction for the paper

Components	$E_1$ (GPa)	$E_2$ (GPa)	$\nu_{12}$ (-)	$G_{12}$ (GPa)	$G_{23}$ (GPa)
UD – HR40/R367-2	180	5	0.28	3.2	2.4
Nomex® paper	4.16	3.3	0.24	1.5	1.0

**Table 2.** Elastic properties of Mixed filled Resin Insert, pads and rollers (isotropy)

Component	E (GPa)	$\nu$ (-)
Mixed filled Resin Insert	1.7	0.3
Polyethylene	0.5	0.4
Steel	210	0.3

**Table 3.** Strength properties of components

Mixed filled Resin Insert [22]	
Failure modes	Maximum stress (MPa)
Compressive strength	-41
Shear strength	25
Nomex® paper [15]	
Failure modes	Maximum stress (MPa)
Compressive strength ( $\sigma_{XX}^F$ )	-105
Compressive strength ( $\sigma_{YY}^F$ )	-90
Shear strength ( $\sigma_{XY}^F$ )	44

**Table 4.** Main maximal stresses values in components from numerical simulation (applied force: 5000 N)

Mixed filled Resin Insert		
Failure mode	Stress (MPa)	Safety factor
Compressive ( $\sigma_{XX}$ )	-8	5
Compressive ( $\sigma_{YY}$ )	-10	3.5
Shear ( $\sigma_{XY}$ )	7	3.5
Nomex® paper		
Failure mode	Stress (MPa)	Safety factor
Compressive ( $\sigma_{XX}$ )	- 22	4.5
Compressive ( $\sigma_{YY}$ )	- 45	2
Shear ( $\sigma_{XY}$ )	15	3

**Table 5.** Experimental protocol for quasi-static tests with fully instrumented specimens. The X stand for a load-unload cycle undergone. The red values indicate the load at failure.

Sample	Cycle 1	Cycle 2	Cycle 3	Cycle 4	Cycle 5	Cycle 6	Cycle 7	Cycle 8
	2400 N	3150 N	3450 N	3950 N	4250 N	4450 N	4650 N	4850 N
HR8_1	X	X	X	X	X	X	X	4830 N
HR7_2	X			X	X	X	X	
HR7_1				X	X	X	X	4537 N

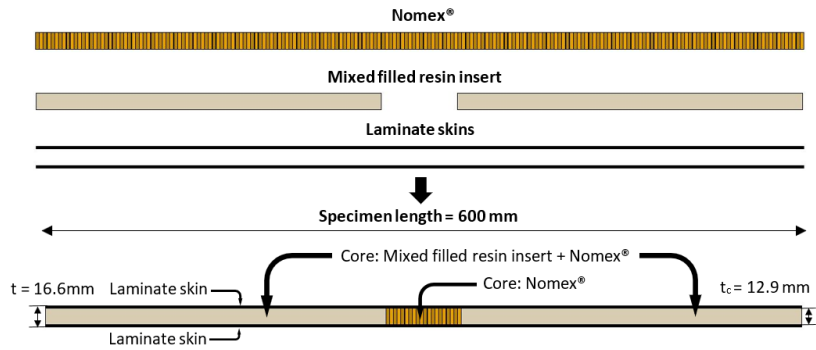


**Figure 2.** Numerical model - Description of the assembly

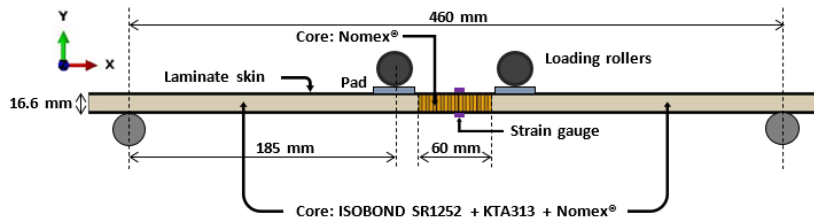


**Figure 1.** Simplified drawing of the four-point bending test fixture

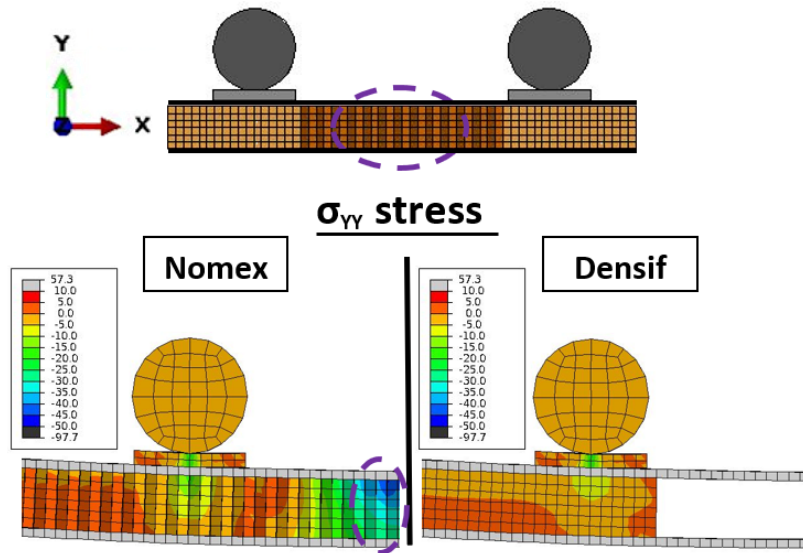


**Figure 3.** Normal stress distribution (in MPa) in the Y direction for both core components under loading rollers and in the centre of specimen (left: Nomex® paper, right: mixed filled resin insert). The ellipses highlight the localization of the maximum values where safety factor is around 2

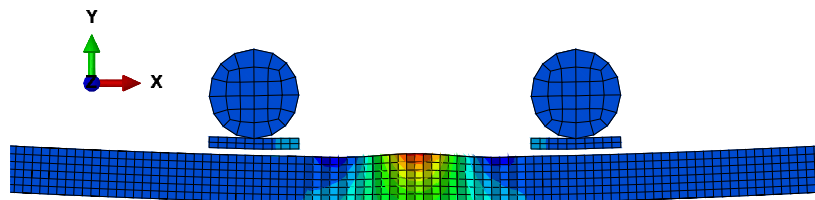


**Figure 4.** First buckling mode from finite elements calculation (face wrinkling)

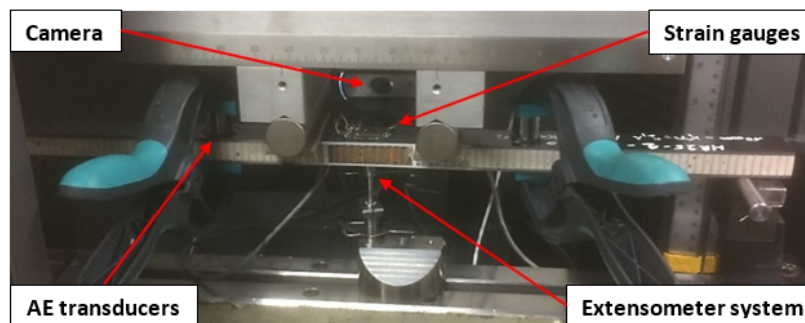


**Figure 5.** Experimental four-point bending set-up with instrumentation

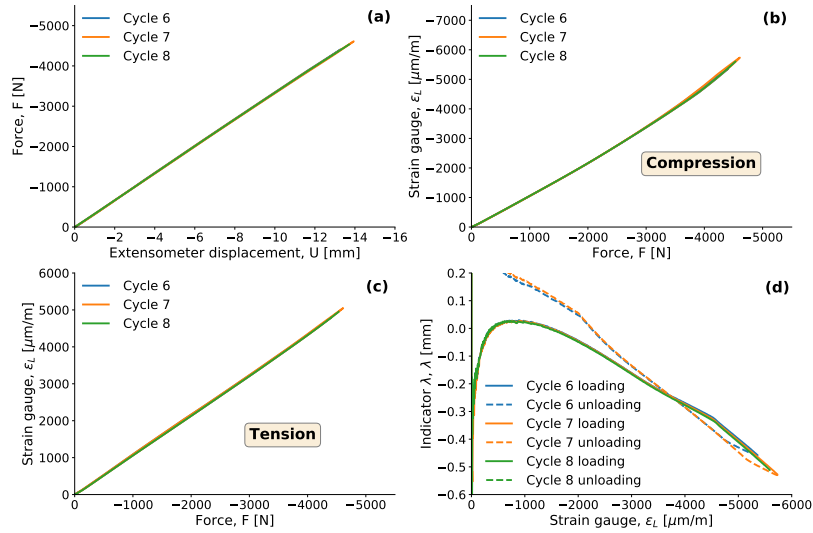


**Figure 6.** Main displacement, load and strain signals measured during the cycles on the HR7\_1 specimen - (a) force-displacement curves ; (b) compressive strain-force curves ; (c) tensile strain-force curves ; (d) Indicator  $\lambda$ -compressive strain curves - of the bending tests for the last three cycles

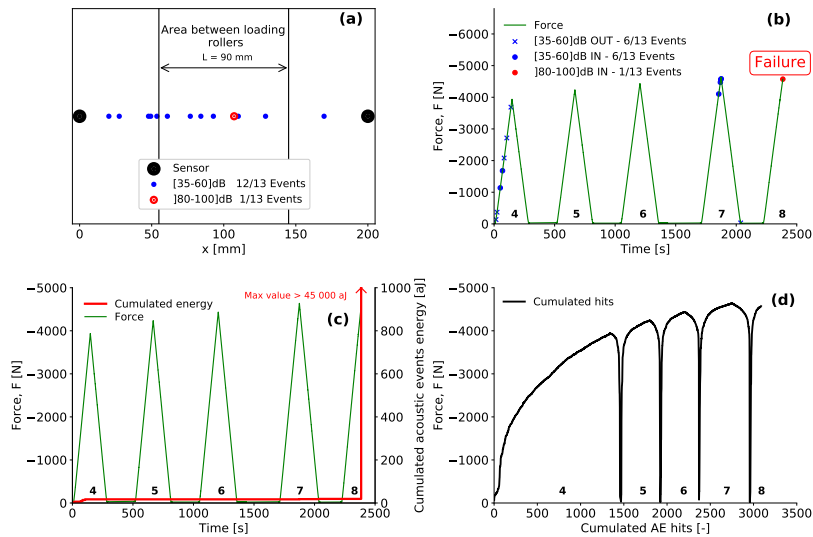


**Figure 7.** Main acoustic emission signals recorded during the cycles on the HR7\_1 specimen (a) spatial localization of events ; (b) load localization of events (OUT: outside the sensors area, IN: inside the sensors area); (c) correlation between force and cumulated energy ; (d) force-cumulated hits

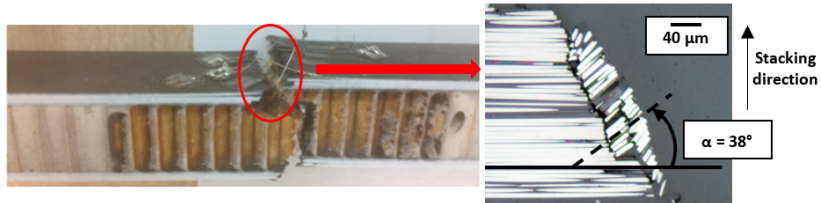


**Figure 8.** Fracture surface of HR7\_1 specimen (left) macroscopic fracture, (right) kinking-bands observed by optical microscopy

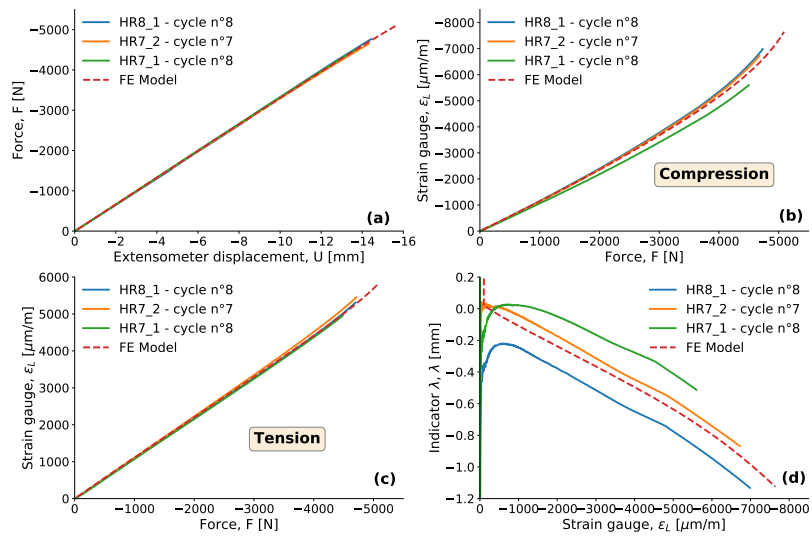


**Figure 9.** Main displacement, load and strain signals measured during the last three cycles of each specimen and for numerical modelling

